Understanding High-Yield Catalyst-Free Growth of Horizontally Aligned Single-Walled Carbon Nanotubes Nucleated by Activated C_{60} Species

Imad Ibrahim,[†,‡] Alicja Bachmatiuk,[†] Daniel Grimm,[†] Alexey Popov,[†] Sami Makharza,[†] Martin Knupfer,[†] Bernd Büchner,[†,§] Gianaurelio Cuniberti,[‡] and Mark H. Rümmeli[†,§,*]

[†]IFW-Dresden e.V., PF 270116, 01171 Dresden, Germany and [‡]Institute for Materials Science and Max Bergmann Center of Biomaterials and [§]Department of Physics, Technische Universität Dresden, D-01062 Dresden, Germany

ABSTRACT Our understanding of the catalyst-free growth of single-walled carbon nanotubes by chemical vapor deposition is limited. Toward improving our knowledge base, we conducted systematic investigations into the initial preparation of C_{60} fullerenes as nucleation precursors for single-wall and even double-wall carbon nanotube fabrication. The role of the dispersing media is shown to be crucial and is related to the initial fullerene cluster size. Oxygen-based groups, in particular, epoxy groups, are shown to be vital prior to actual growth. Moreover, the presence of oxygen groups during the growth phase is necessary for tube development. We also demonstrate the possibility of fabricating the tubes in crossbar configurations with bespoke crossing angles in a single synthesis step, unlike other routes which require at least two synthesis steps. The systematic studies significantly advance our understanding of the growth mechanisms involved in all-carbon catalyst-free growth of single- and double-walled carbon nanotubes.

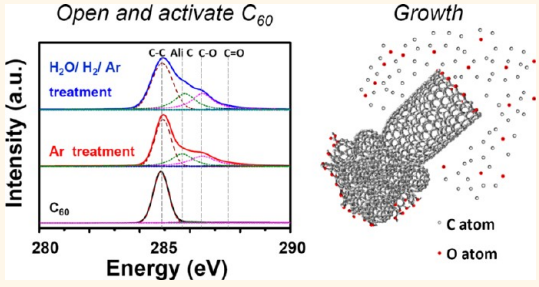

KEYWORDS: catalyst-free · carbon nanotubes · C_{60} · nucleation · growth · CVD

Extraordinary properties of the single-walled carbon nanotubes (SWNTs) have stimulated an enormous amount of research toward the realization of SWNT-based products for different applications ranging from nanocomposites to nanoelectronics.[1−5] Their high mobility, exceedingly good current-carrying capacities, and ability to be either semiconducting or metallic render them ideal building blocks for nanoelectronics.[6,7] For nanoelectronic applications, either individual or parallel aligned SWNTs are advantageous.[7] There is also a drive to fabricate well-oriented SWNTs either horizontally aligned or in crossbar formation for further processing into arrays of complex devices. Moreover, closely packed arrays of parallel SWNTs are required in order to sustain the relatively large currents found in high-frequency devices.[8] Two key areas that still require further development before the realization of large-scale nanoelectronics are the reproducible control of the nanotubes' spatial position/orientation and chiral management.[9] In terms of nanotube orientation, different techniques have been developed for the fabrication of horizontally aligned SWNTs with either postgrowth strategies (*e.g.*, dielectrophoresis and Langmuir−Blodgett approach)[10−12] or direct growth (*e.g.*, chemical vapor deposition (CVD)).[13,14] These techniques suffer some drawbacks, namely, because they are synthesized using catalyst particles (metals or nonmetals) and the catalyst material can contaminate the tubes and affect their intrinsic properties.[15,16] Moreover, catalyst material can diffuse in devices which can lead to device failure. This makes catalyst-assisted SWNT fabrication somewhat incompatible with Si-based technology.[17] Thus, the catalyst-free synthesis of aligned SWNTs is very attractive. To this end, various all-carbon routes have been developed, for example, SWNTs grown from diamonds[18] and cloning open-ended SWNT seed pieces.[19] It is also possible to use opened fullerenes as nucleation sites for SWNT growth

* Address correspondence to m.ruemmeli@ifw-dresden.de.

Received for review September 11, 2012 and accepted November 27, 2012.

Published online November 27, 2012
10.1021/nn304189y

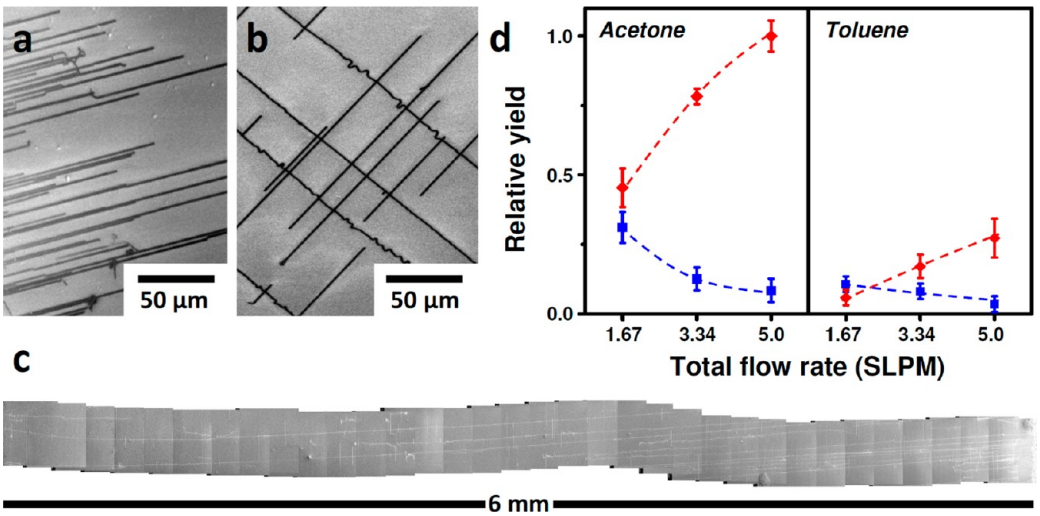

Figure 1. SEM micrographs of fullerene-nucleated aligned SWNTs (a) lattice-oriented, (b) crossbar array, and (c) long (6 mm) flow-oriented SWNTs. (d) Relative yield dependency of the SWNTs on the total flow rate for fullerenes dispersed in acetone and toluene (diamonds represent flow-oriented tubes, and squares represent lattice-oriented tubes).

using CVD.[20,21] The Rao group[20] used opened C_{60} and C_{70} fullerenes as nucleation centers, while the Yu group[21] used exohedrally functionalized fullerenes, which they argued were easier to open. However, functionalized fullerenes are costly and are not an ideal choice to use as nucleation centers for the catalyst-free growth of SWNTs. It has been argued that growth from fullerene-nucleated tubes occurs by surface diffusion. Nonetheless, our understanding of all-carbon growth of SWNTs is very limited; in particular, how carbon addition takes place at the open growing end of a tube is unclear. Yu *et al.*[21] argue that oxygen-terminating groups are not important for growth; however, this stands in contrast to other studies arguing that oxygen-based groups are crucial for growth.[22−26] Indeed, the work by Lin *et al.*,[23] in which functionalized graphite terminated with oxygen-rich groups yielded carbon nanotubes under conventional CVD conditions and untreated graphite did not yield carbon nanotubes, is an important case in point.

In this study, we systematically investigate each synthesis step of catalyst-free horizontally oriented SWNTs nucleated from pure C_{60} fullerenes to gain insight into the growth mechanisms involved. This includes investigating the role of the solvent used to disperse the C_{60}, the pretreatment steps to open and functionalize (activate) the fullerenes, and aspects of the CVD growth process itself. Our investigations show that it is possible to obtain catalyst-free grown SWNTs in high yield. We also show for the first time that fullerene-based nucleation can also lead to double-walled carbon nanotube (DWNT) production. Moreover, we demonstrate that it is possible to grow crossbar arrays of aligned SWNTs in a single step. As far as we are aware, all other crossbar techniques require at least two processing steps.[7,27,28]

RESULTS AND DISCUSSION

Panels a−c of Figure 1 show typical micrographs of aligned SWNTs grown over stable temperature (ST)-cut quartz substrates using our CVD route. Depending on the gas flow rate, one can have single direction aligned tubes (panels a,c) or crossbar aligned tubes (panel b). In the case of single direction aligned SWNTs (panel a), the gas flow rates during synthesis are relatively high so that the tube orientation/alignment is dominated by the interaction between the ST-cut quartz surface lattice and the growing tube, viz. lattice orientation.[14] By reducing the flow sufficiently, a laminar flow can be established. Under these conditions, the growing tubes fly just above the substrate surface and align themselves in the direction of the gas flow and are referred to as flow orientation.[30] However, if the flow is not too low, tube alignment by lattice orientation persists. Under these conditions, both flow orientation and lattice orientation occur in tandem. Thus, by altering the angle between the gas flow and the lattice orientation, one can form crossbar aligned SWNTs with tunable angles in a single synthesis step (see Figure 1b and Figure S1 in the Supporting Information). This stands in contrast to other routes which require two synthesis steps to obtain crossbar aligned tube formation.[27,28]

One can also tailor the relative yield of lattice- and flow-oriented tubes as highlighted in Figure 1d. Note that yield is defined as the number of SWNTs per unit area, while the relative yield is obtained by normalizing the yields to the highest achieved yield for a given case. When reducing the flow rate sufficiently, lattice orientation can be significantly reduced since now lamellar flow conditions enable most of the catalyst particles and emerging tube to float just above the substrate surface. Thus any interaction with the surface lattice is

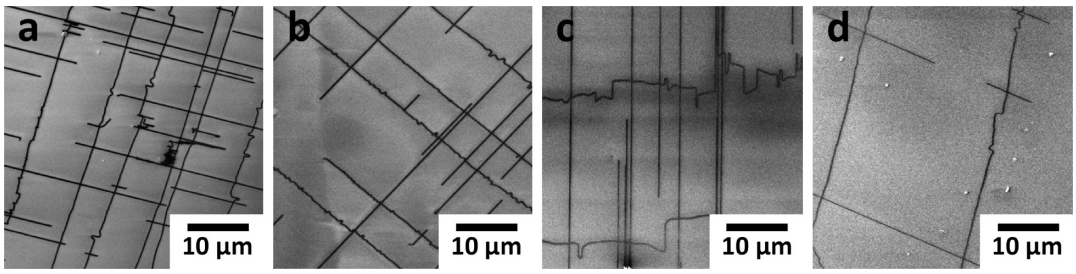

Figure 2. Representative SEM images for the aligned SWNT yield nucleated from fullerenes initially dispersed in (a) acetone, (b) ethanol, (c) methanol, and (d) toluene.

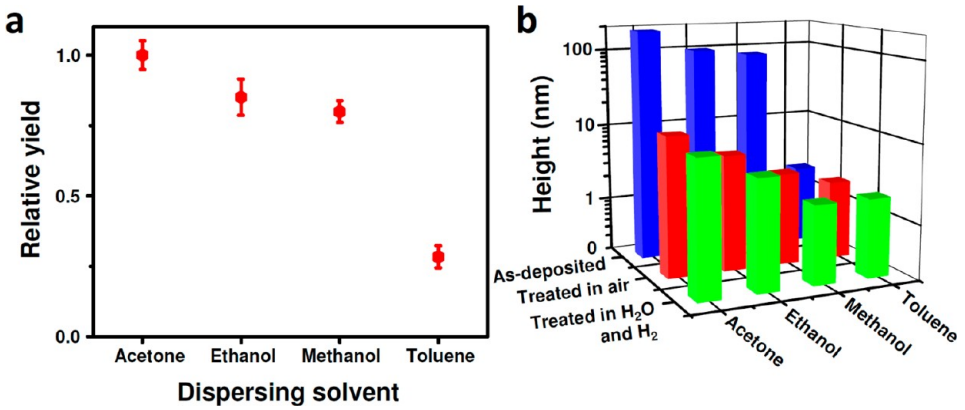

Figure 3. (a) Relative yield dependency on initial fullerene dispersing media. (b) Diameter (height) distribution of the as-deposited fullerene clusters from different dispersing media and then later oxidized in air and then after air oxidation and H_2O/H_2 treatment.

removed, and hence lattice orientation does not occur. Flow-oriented tubes can grow over vast distances because friction forces are minimized as illustrated in panel c in which SWNTs over 6 mm long are demonstrated. It is also argued that higher growth rates occur with flow-oriented growth as opposed to lattice-oriented growth.[7] Lattice-oriented tubes are on average 0.1 mm long. For further discussion, we present data with a constant flow (1.67 standard liter per minute, slpm) for all samples that yield a crossbar aligned network of SWNTs.

Clear differences in the yield can be observed between the different media used to disperse the fullerenes prior to deposition on the ST-cut quartz substrate. The two extreme examples are acetone and toluene, as depicted Figure 1d. We also explored the use of ethanol and methanol. Figure 2 shows representative scanning electron microscopy (SEM) micrographs for the four explored dispersing media. The change in yield is easy to see and is quantified in Figure 3a. At first glance, one might anticipate there to be a link between yield and fullerene solubility in the solvent of choice. If this were directly so, then according to Ruoff *et al.*,[29] the poorest solubility should occur for methanol, then ethanol, followed by acetone, and finally toluene. Toluene is known to be one of the best solvents to disperse C_{60}, and so one can anticipate an almost unimolecular distribution to form in the dispersion and subsequent deposition of C_{60}. In contrast, dispersion in the other media is not so effective and clusters tend to form; that is, the solubility of C_{60} in acetone, ethanol, and methanol is very low.[29] Figure 3b quantifies this information, and one can clearly observe the relative changes in C_{60} cluster size. The cluster sizes increase markedly for methanol and ethanol, and then acetone has the largest cluster size. A clear correlation between cluster size and yield can be observed; namely, larger cluster sizes lead to larger SWNT yields. The higher CNT yield achieved when using fullerenes dispersed in acetone could, in part, be attributed to the destruction of the double O═C bond into a single bond due to the sonication process. This would allow attachment of an acetone molecule to the fullerene. This makes opening such a fullerene easier and hence increases the number of caps formed. This can explain why acetone, despite having a solubility between toluene and methanol, has the highest yield. Further data on the cluster size evaluation are presented in Figure S3 in the Supporting Information.

To better comprehend this connection, we need to look at the steps involved in the applied CVD synthesis route. Initially, a two-step pretreatment step is employed. In the first, an oxidation treatment is applied, and this is followed by a short exposure to H_2O (2 min), followed by a brief exposure to H_2 (3 min). The first oxidation step is crucial, as shown by Yu *et al.*, to open

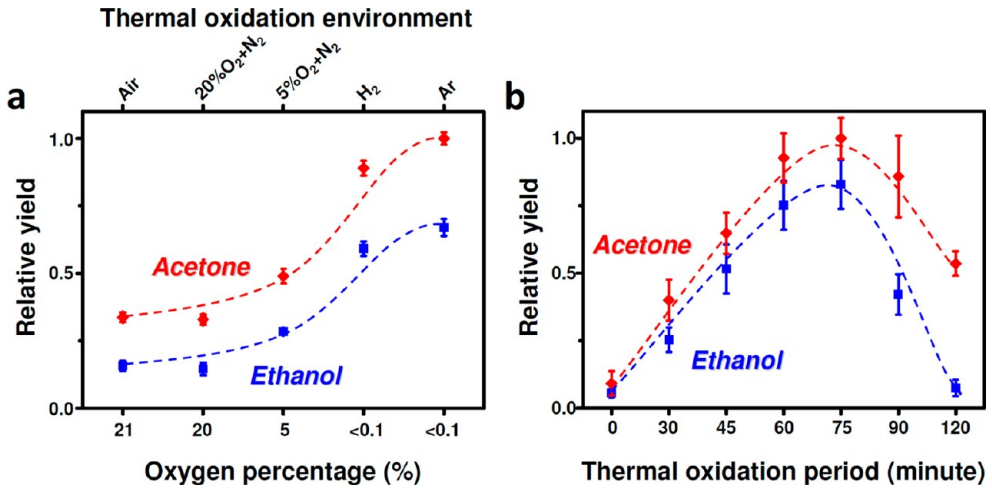

Figure 4. Relative yield of carbon nanotube dependency on (a) thermal oxidation environment and (b) thermal oxidation period. In both a and b, diamonds represent the tubes nucleated from fullerene dispersed in acetone and squares represent tubes nucleated from fullerenes dispersed in ethanol. Further information on the oxidation process is available in Figure S5 in Supporting Information.

up the fullerenes to provide hemispherical caps which then serve as the nucleation sites for continued tube growth.[21] One would anticipate the oxidation process to diminish the cluster size. In practice, this is exactly what happens, as can be seen in Figure 3b. In this case, the pretreatment consisted of heating the deposited fullerenes in air at a temperature of 500 °C for 75 min. After the oxidation process, the hemispherical caps need to be activated for growth, and this is achieved in the secondary step by exposure to H_2O/H_2. This step functionalizes the dangling bonds at the open ends of the hemispherical caps, thus activating them for growth. The secondary treatment does not significantly reduce the size of the clusters, as can be seen in Figure 3b. The H_2O/H_2 treatment is argued to also remove unwanted amorphous species.

Regarding the initial pretreatment step to open the fullerenes by oxidation, this process is obviously a delicate process, and not all oxidized fullerenes will yield hemispherical caps. To optimize the process, we explored the use of oxidation environments with differing oxygen content. The environments explored were air, synthetic air, nitrogen with 5% oxygen, hydrogen, and argon. In the latter two cases, an oxygen detector was used. The oxygen limits were below 0.1% (detection limit). For all of the investigated dispersing media, the resultant yield of SWNTs was best when oxidizing using Ar in the pretreatment step. In short, as the oxygen content is increased, the SWNT yield decreased. This behavior is demonstrated for samples prepared using acetone and ethanol to disperse the fullerenes in Figure 4a. The relative yield between the four explored dispersing media did not change between pretreatments, and this is concomitant, again, with the cluster size (both before and after pretreatment). See Figure S4 in the Supporting Information for more details. We also explored different pretreatment times. In general, the yield increases with treatment time up to an oxidation time of *ca.* 75 min, after which the yield drops (Figure 4b). The drop in yield can be attributed to excessive oxidation; that is, most of the fullerene clusters have been burnt away. With regard to the optimum oxidation time, the reasons are not so clear because, by this time, the cluster sizes have been reduced by an order of magnitude.

As just mentioned, the pretreatment steps likely functionalize the fragments of opened fullerenes. To investigate this process in greater detail, we employed the use of infrared (IR) and X-ray photoemission spectroscopies (XPS). We begin with the IR data between 1000 and 3700 cm^{-1}. In all samples (the starting material, the sample after the initial pretreatment (oxidation in Ar), and after a secondary treatment), a variety of functional groups can be observed. These include C−O, O−H, C═O, C−OH, and COOH groups. The relative intensity of each varies from sample to sample and across the different dissolution solvents explored. Some basic trends can be observed though. As a general rule, the intensity of C═O bands (*ca.* 1500 and 1700 cm^{-1}) relative to that of the C−O band (*ca.* 1200 cm^{-1}) is reduced after the initial pretreatment in Ar. After the secondary H_2O/H_2 treatment, the relative strength of the C═O bands is increased, and in addition, the O−H bands (*ca.* 1400 and 3600 cm^{-1}) are stronger. This confirms the functionalization efficiency of the H_2O/H_2 treatment. Variations between samples prepared using different solvents for fullerene dispersion can also be observed. In particular, the relative intensity ratio of C−O and C═O bands changes such that the C−O/C═O ratio increases as one goes from toluene, to methanol, to ethanol, and finally to acetone (see Figure S6). This trend is concomitant with the final yield of CNTs. With regards to the functionalization observed in the starting material, this presumably

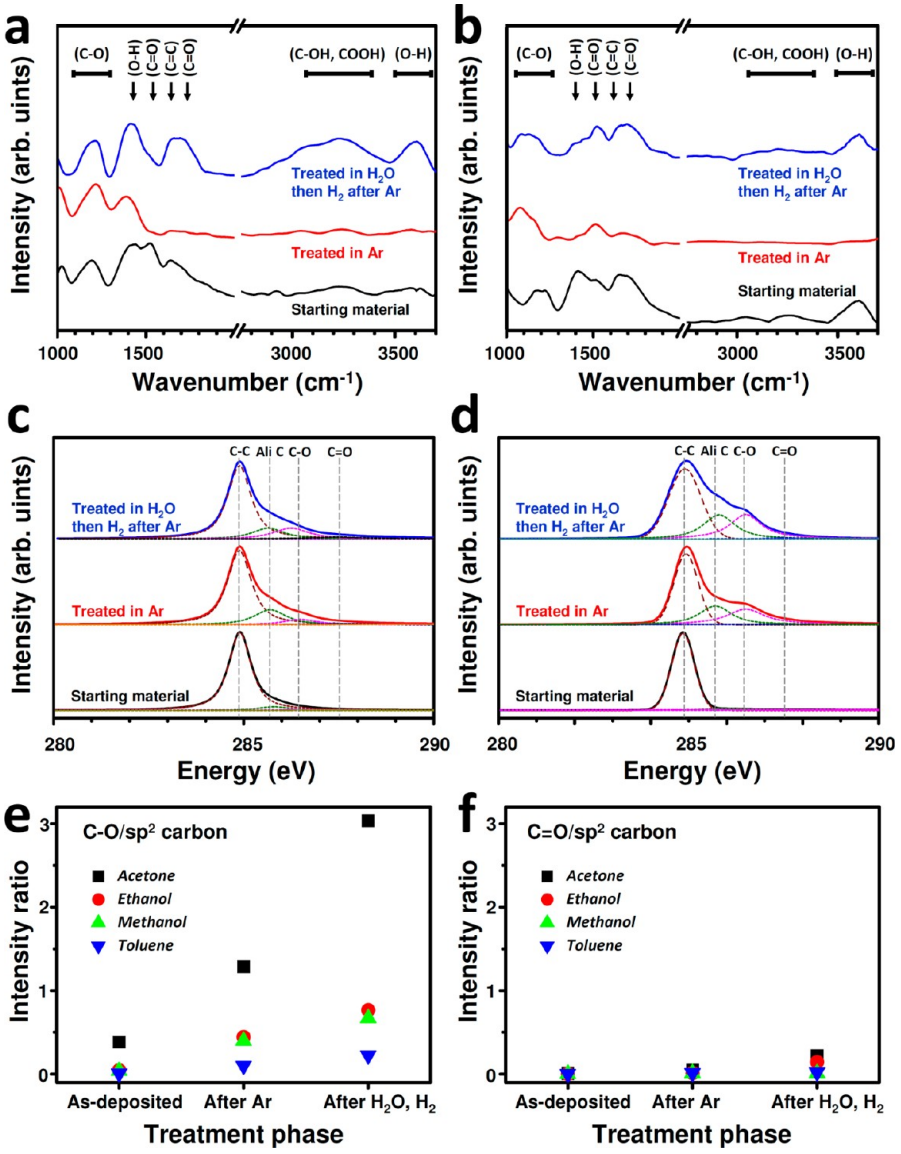

Figure 5. FTIR spectra for the as-deposited material, Ar-pretreated, and Ar-pretreated followed by H_2O/H_2 pretreatments from fullerenes dispersed in (a) toluene and (b) ethanol. C1s core level spectra as well as deconvoluted peaks corresponding to different functional groups for the as-deposited, Ar-treated, and Ar-treated followed by H_2O/H_2 pretreatments from fullerenes dispersed in (c) toluene and (d) ethanol. (e,f) C−O and C═O ratios relative to sp^2 C intensities for fullerenes dispersed in the different dispersing media after all pretreatments.

arises during the ultrasonication treatment prior to deposition.

To further evaluate the functionalization of the fullerenes upon exposure to the pretreatment steps, we employed XPS. Two examples for the C1s edge spectra are provided in panels c and d of Figure 5 for toluene and ethanol, respectively. Corresponding O1s edge spectra are provided in Figure S7 in the Supporting Information. Both the C1s and O1s edges indicate the presence of sp^2 carbon (284.9 eV) and functional groups, namely, aliphatic carbons (285.7 eV), C−O (286.3 eV), and C═O (287.7 eV)[31] after deconvoluting the peaks using XPSPeak 4.1. The data show that, for all of the dispersing media investigated, the fullerene clusters of the C−O and C═O peaks increase relative to the sp^2 peak after each pretreatment step, more so for the C−O peak than the C═O peak, as shown in Figure 5e,f. In addition, the relative intensity of the C−O and C═O peaks increases as one goes from toluene, to ethanol, and to methanol (similar), and finally to acetone. Moreover, the ratio of the C−O to C═O peaks increases in the same manner concomitant with the FTIR observations (see Figure S8 in the Supporting Information).

After the pretreatment steps, the growth reaction is applied to grow carbon nanotubes from the opened and activated fullerenes. We investigated two feedstocks: methane (CH_4) and ethanol (CH_3CH_2OH). When using methane, despite investigating various synthesis conditions (*e.g.*, temperature and flow), we never

observed the growth of SWNTs. When using ethanol, SWNTs are easily obtained. To investigate the as-grown SWNTs while still on the substrate, we employ atomic force microscopy (AFM) since one can gain insight into the heights (diameters) of the tubes. The data show that the tube diameters lie in the range of 0.7 and 1.4 nm. A more thorough statistical evaluation suggests a quantized variation in the SWNT mean diameter, most notably between 0.7 and 1.0 nm. This quantization, which is not observed when using metallic or nonmetallic catalyst particles, is illustrated in Figure S9 in the Supporting Information and is similar to observations by Yu *et al.*[21] They argued that this quantization arises because partial hemispherical fragments from oxidized fullerenes that formed during the pretreatment steps can merge, forming caps that are larger than a C_{60} hemisphere (0.7 nm). This same argument may help explain why the optimal oxidation time (pretreatment), which burns away a lot of the cluster material, is rather long. In other words, while on one side the oxidation treatment burns, opens, and etches the fullerenes, some fragments are able to merge in this process as a competing process. Another feature we often observed was a bulbous-like feature at the end of a tube. Presumably, these are the clusters from which a tube stems and grows. A detailed analysis of these bulb heights shows that they range between 2 and 10 nm and shows no correlation to the SWNT diameters, as illustrated in Figure S10 of the Supporting Information.

AFM cannot unequivocally identify or distinguish individual tubes and small bundles. Hence we employed transmission electron microscopy (TEM) and Raman spectroscopy to confirm that the structures are SWNTs. The TEM studies confirm that the vast majority of tubes are SWNTs (see Figure 6c,d). Occasionally, a DWNT can be observed (panel d). To the best of our knowledge, this is the first observation of catalyst-free grown DWNTs.

The use of Raman spectroscopy also allows one to identify SWNTs through a sharp G mode (*ca.* 1600 cm^{-1}), D mode (*ca.* 1400 cm^{-1}), a high intensity ratio of the G to D modes, and finally the well-known radial breathing modes (RBM). A typical example is provided in the Supporting Information in Figure S11. One can obtain diameter information from the RBM modes according to the following equation:[32]

$$d_t = \alpha/\omega_{RBM}, \text{ where } \alpha = 248 cm^{-1} nm$$

where $\alpha = 248$ and ω_{RBM} is the Raman shift (cm^{-1}). Since the RBM values are dependent on the excitation laser wavelength, we investigated the samples for three wavelengths, 780, 633, and 532 nm (see Supporting Information, Figure 10b). The Raman spectroscopic data indicate the presence of SWNTs ranging between 0.7 and 1.5 nm. This is in good agreement with the AFM

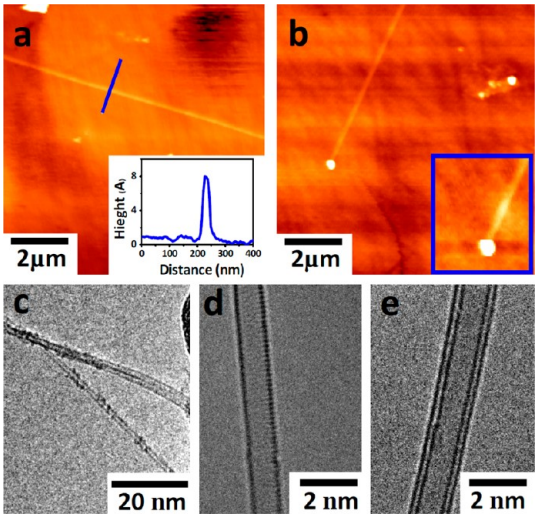

Figure 6. (a) AFM image for a lattice-oriented SWNT. Inset: Height profile of the tube taken at the place indicated by the blue line. (b) Typical AFM image for fullerene-nucleated SWNTs showing a cluster at the end of the tube. Inset: Magnified AFM image of the cluster at the end of the nanotube. (c–e) TEM micrographs of SWNTs and DWNTs produced by the all-carbon catalyst-free CVD synthesis route.

evaluation. The RBM corresponding to large diameter tubes (*i.e.*, 1.4–1.5 nm) could arise from DWNTs with inner tubes of *ca.* 0.7 nm.

From the obtained data, one can start to build a picture of the processes involved when growing SWNTs from fullerenes. First, the type of solvent used to disperse the fullerenes prior to deposition affects the size of the fullerene cluster deposited on the ST-cut quartz substrate such that larger clusters yield more SWNTs. This is easily interpreted as larger clusters providing a larger number of fullerenes that can potentially be opened and provide a nucleation cap for carbon nanotubes. Fragments unsuitable for nucleation may be able to merge with other fragments, also providing a nucleation cap.[21] The investigation on the pretreatment oxidation process to open the fullerenes is a delicate process. Moreover, by optimizing the oxidation time and environment efficient cap, production can ensue. It could also be that the choice of solvent to disperse the fullerenes can exohedrally functionalize them, which may make them more susceptible to opening. The spectroscopic data highlight the functionalization role of the second pretreatment step, in which the opened fullerenes are subjected to H_2O vapor and then H_2. Indeed, the spectroscopic data suggest epoxy (C–O) groups are relatively more abundant than carbonyl (C=O) groups and more importantly that the level of epoxy and carbonyl functionalization is lowest for fullerenes dispersed in toluene and greatest for fullerenes dispersed in acetone. Samples dispersed in ethanol or methanol lie in between. These trends in functionalization follow the relative yields of SWNTs obtained from different C_{60} dispersing

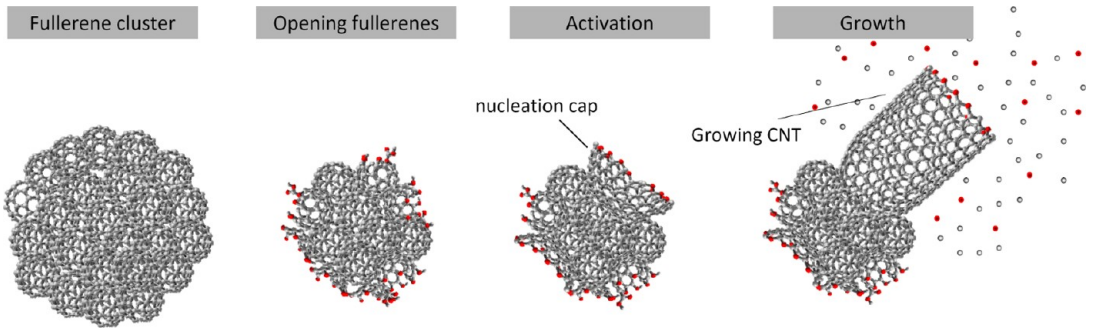

Figure 7. Schematic illustration of the proposed mechanisms for the pretreatments/activation and growth steps for carbon nanotubes nucleated from activated fullerene species.

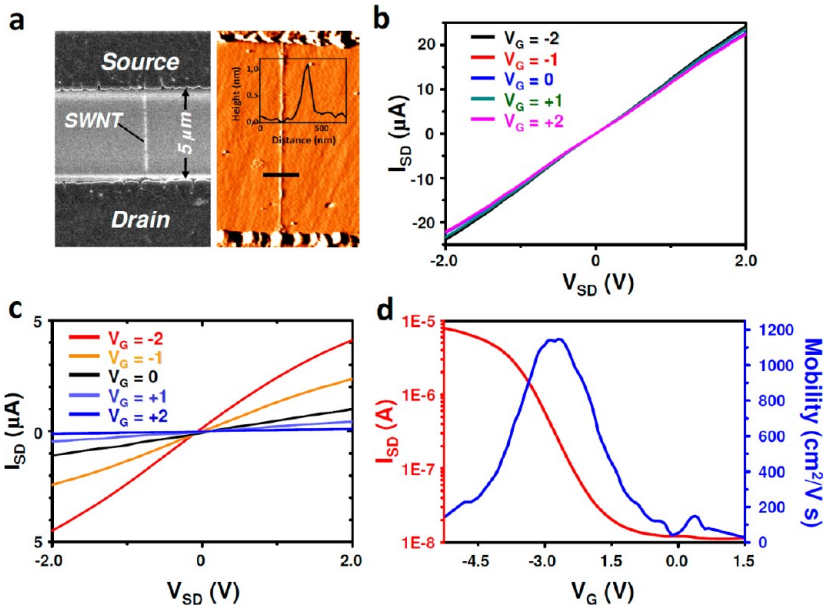

Figure 8. (a) SEM (left) and AFM (right) micrographs of a FET prior to top gate fabrication. The source−drain channel length is 5 μm, and the tube height is 1.1 nm (see inset). Representative (b) *IV* characteristics of a metallic SWNT. (c) Representative current−voltage (*IV*) characteristic and (d) transfer characteristic (dependence of I_{SD} and mobility on the gate voltage (V_G)) for a semiconducting SWNT FET.

media used to disperse them and suggest that they are crucial to activating open fullerene caps for SWNT growth during the CVD reaction. The FTIR and XPS data suggest that epoxy groups are most important. Once the fullerenes have been opened and activated nucleation caps formed, the CVD growth process takes place. The choice of feedstock seems important in that with methane as the C source no SWNTs are obtained while with ethanol, under optimized conditions, abundant SWNTs can be found. This again suggests that oxygen-based groups are relevant. This is in keeping with other studies that suggest oxygen-based groups are important for both catalyst and catalyst-free growth of CNTs.[22−26] How oxygen is important for growth is not exactly clear; however, the spectroscopic data on the activation process (pretreatment) provide a hint that epoxy groups are key. From this, it is reasonable to infer that an oxygen atom bridging two carbon atoms may be able to break one of its bonds, enabling a new carbon unit (*e.g.*, C, C_2 C_3...) to enter. Once the new carbon unit has inserted itself onto the growing tube end, the oxygen atoms can rebond and saturate a dangling bond. Of course, in this process, both oxygen bonds can break, releasing the oxygen, and so new oxygen-based groups (*e.g.*, CO) need to be available to replenish oxygen at the end of a growing tube. This could explain the need for a feedstock that is able to supply both C and O species. Oxygen species, for example, OH radicals, can also help prevent amorphous carbon buildup that could block growth at the open end of a SWNT. Figure 7 provides a schematic illustrating the different steps involved in the opening and activation of C_{60} to provide nucleation sites for subsequent SWNT growth. In the case of DWNTs, it is probable that fullerene fragments forming nucleation caps are able to overlap each other in a manner enabling two nucleation caps to form with one residing inside the other, as shown schematically in Figure S12. Of course, this is statistically less favorable and explains why SWNTs dominate in the samples.

We also investigated the transport characteristics of field effect transistor (FET) devices fabricated using our catalyst-free grown tubes. More than 50 devices were produced. They were fabricated by first forming source and drain contacts (see Figure 8a) and then placing an Al_2O_3 top gate. Greater details on the fabrications steps are available in the Methods section. Initial *IV* characterizations showed about two-thirds of the devices have semiconducting tubes and the rest were metallic. A typical example of the *IV* characteristics for metallic and semiconducting tube devices for different gate bias is shown in panels b and c, respectively. Further examples are available in the Supporting Information. The metallic tube devices show a linear *IV* response (panel b) with no gate dependence, while the semiconducting tubes show the current (I_{SD}) beginning to saturate at higher voltages. The transfer characteristics and mobility of the semiconducting device are shown in panel d. The semiconducting SWNTs conduct well with negative gate voltages (up to 4 μA at $V_G = -2$ V) and then become almost insulating at high positive voltages, indicating a p-type semiconducting tube.[33] The mobility of the device is also shown in panel d and is determined using the following equation:[34]

$$\mu = \frac{L}{V_{SD}C_t}\frac{dI_{SD}}{dV_G}$$

where L is the device channel length, V_{SD} denotes the source−drain voltage, dI_{SD}/dV_G is the source−drain derivative with respect to the gate voltage, C_t is the gate capacitance per unit length of the CNT and is calculated using

$$C_t = \frac{2\pi\varepsilon_{ox}}{\ln(4t_{ox}/W)}$$

where ε_{ox} and t_{ox} denote the effective dielectric constant and thickness of the insulating layer separating the CNT from the gate electrode, respectively. The insulating layer used in this study was Al_2O_3, for which ε_{ox} and t_{ox} are 9.1 ε_o and 50 nm, respectively. The diameter of the semiconducting channel (CNT) is given by W. For the device shown in Figure 8c, the mobility is around 1100 $cm^2\ V^{-1}\ s^{-1}$. The transfer characteristics of a number of other devices fabricated using catalyst-free grown SWNTs are shown in Figure S13 in the Supporting Information. The mobility of these devices ranges from 680 and 1100 $cm^2\ V^{-1}\ s^{-1}$, which is highly comparable with catalyst-grown SWNT-based FETs.[33−37] The devices shown in this work exhibit a resistance in the range of 50−150 kΩ. This relatively high resistance can be attributed to backscattering and contact effects. This results in a saturation in the I_{SD} at high V_{SD} (see Figure S15 in Supporting Information).[38−44]

TABLE 1. Flow Rates Introduced into the CVD Oven in the Growth Phase

	H_2 (slpm)	Ar (slpm)	Ar bubbled through ethanol (slpm)
flow-oriented SWNTs	1.5	0.07	0.10
crossbar SWNT	3.0	0.13	0.21
lattice-oriented SWNTs	4.5	0.20	0.32

CONCLUSION

In summary, we have systematically investigated the initial preparation steps, pretreatment steps, and growth of catalyst-free grown carbon nanotubes using C_{60} as nucleators. The data show that large initial fullerene clusters help by providing more nucleation sites. Careful oxidation steps to open and functionalize the fullerenes are shown to be crucial, and moreover, oxygen-based functional groups, in particular, epoxy groups, appear to be important. Oxygen remains important during growth, as no growth occurs when using precursors devoid of oxygen. The as-synthesized tubes are mostly SWNTs; however, we also show that it is possible to obtain DWNTs. Moreover, crossbar array formation in a single synthesis step is also demonstrated. These systematic studies significantly advance our understanding of the growth mechanisms involved in catalyst-free growth of single- and double-walled carbon nanotubes.

METHODS

To prepare the fullerenes on the surface of the support, nominal amounts of C_{60} fullerenes were dispersed in 10 mL of different dispersing media, namely, toluene, acetone, ethanol, and methanol, and then ultrasonicated overnight to ensure better dispersion. Thereafter, a drop of the solution was drop coated on the support surface. ST-cut single-crystal quartz substrates were used as the support (10 mm diameter, 0.5 mm thickness, angle cut 38° 00′, seeded, single side polished from Hoffman Materials, LLC). The ST-cut quartz substrates were subjected to thermal annealing in air at 750 °C for 15 h prior the fullerene drop coating. Thermal treatment leads to a smoother substrate surface, which enhances the yield and alignment degree of the grown tubes.[14] The coated samples were inserted to the middle of 2.54 cm purpose-built horizontal tube furnace where they were subjected to thermal oxidation by heating in various environments: air, synthetic air, Ar, or H_2 for between 10 and 120 min. The temperature varied from 400 to 500 °C. A further pretreatment ensued prior to the CVD by heating in water vapor (0.17 slpm Ar bubbled through water) for 2 min and then heating in hydrogen (0.75 slpm) for 3 min at 900 °C. Thereafter, the optimized CVD reaction was conducted in a gaseous environment consisting of hydrogen, Ar, and Ar bubbled through ethanol. The CVD reaction is run for a period of 20 min at a temperature of 900 °C. The gas flow rates varied depending on the desired alignment process, as shown in Table 1.

The as-deposited and treated fullerene clusters and as-produced SWNTs were characterized in terms of their morphology, yield, length, diameter, alignment, and homogeneity using AFM (Digital Instruments Veeco, NanoScope IIIa) in the tapping mode, a SEM (FEI, NOVA NanoSEM 200, with typical acceleration voltage of 3 kV), and TEM (A double Cs corrected JEOL JEM-2010F using an acceleration voltage of 80 kV). The electronic properties and quality of the SWNTs were also characterized using Raman spectroscopy (Thermo Scientific, DXR Smart Raman) with excitation laser wavelengths of 780, 633, and

532 nm. FTIR (Bruker IFS 113 V spectrometer) and XPS were also implemented (the XPS experiments were carried out using a commercial PHI 5600 spectrometer equipped with a monochromatized Al Kα source). The samples characterized with AFM, SEM, and Raman spectroscopy were investigated as-is on the ST-cut quartz substrates without any further preparation. In the case of FTIR and XPS measurements, the material was transferred by scratching the host substrate with KBr substrates and aluminum foil, as these substrates have no response against FTIR and XPS, respectively. For TEM investigations, the as-grown SWNTs were transferred from the hosting substrates onto TEM grid using a protocol described elsewhere.[44] For the electrical measurements, a set of source–drain electrode pairs was fabricated using standard e-beam lithography on the substrates where the nanotubes were as-grown. This was followed by preparation of a 50 nm thick insulating material (Al_2O_3) serving as a top gate oxide. Later, a third electrode (gate) was fabricated with e-beam lithography over the gate. The three electrodes contain a thin layer of Cr (10 nm) followed by 40 nm of Au.

Conflict of Interest: The authors declare no competing financial interest.

Acknowledgment. I.I. and S.M. thank the DAAD; A.B. thanks the Alexander von Humboldt Foundation and the BMBF. A.P. thanks the DFG (grant PO1602/1-1). G.C. acknowledges support from the South Korean Ministry of Education, Science, and Technology Program, Project WCU ITCE No. R31-2008-000-10100-0, and M.H.R. thanks the EU (ECEMP) and the Freistaat Sachsen. The authors thank A. Hofmann for the help in the fabrication of electrodes by EBL.

Supporting Information Available: Representative SEM images of various crossbar arrays of SWNTs are provided. Studies on the fullerene cluster formation for different dispersing media and treatment steps are also given. Moreover, additional XPS, FTIR, and Raman spectra are available. The *IV* and transfer characteristics of different metallic and semiconducting SWNTs, along with the mobility study of the semiconducting tubes, are also given. This material is available free of charge *via* the Internet at http://pubs.acs.org.

REFERENCES AND NOTES

1. Saito, R.; Dresselhaus, G.; Dresselhaus, M. S. *Physical Properties of Carbon Nanotubes*; Imperial College Press: London, 1998.
2. Wen, Q.; Qian, W.; Nie, J.; Cao, A.; Ning, G.; Wang, Y.; Hu, L.; Zhang, Q.; Huang, J.; Wei, F. 100 mm Long, Semiconducting Triple-Walled Carbon Nanotubes. *Adv. Mater.* **2010**, *22*, 1867–1871.
3. Tans, S. J.; Verschueren, A. R. M.; Dekker, C. Room-Temperature Transistor Based on a Single Carbon Nanotube. *Nature* **1998**, *393*, 49–52.
4. Kang, S. J.; Kocabas, C.; Ozel, T.; Shim, M.; Pimparkar, N.; Alam, M. A.; Rotkin, S. V.; Rogers, J. A. High-Performance Electronics Using Dense, Perfectly Aligned Arrays of Single-Walled Carbon Nanotubes. *Nat. Nanotechnol.* **2007**, *2*, 230–236.
5. Chen, Z.; Appenzeller, J.; Lin, Y. M.; Sippel-Oakley, J.; Rinzler, A. G.; Tang, J.; Wind, S. J.; Solomon, P. M.; Avouris, P. An Integrated Logic Circuit Assembled on a Single Carbon Nanotube. *Science* **2006**, *311*, 1735.
6. Rouhi, N.; Jain, D.; Zand, K.; Burke, P. J. Fundamental Limits on the Mobility of Nanotube-Based Semiconducting Inks. *Adv. Mater.* **2011**, *23*, 94–99.
7. Ibrahim, I.; Bachmatiuk, A.; Warner, J. H.; Büchner, B.; Cuniberti, G.; Rümmeli, M. H. CVD Grown Horizontally Aligned Single Wall Carbon Nanotubes: Synthesis Routes and Growth Mechanisms. *Small* **2012**, *8*, 1973–1992.
8. Kocabas, C.; Hur, S.-H.; Gaur, A.; Meit, M. A.; Shim, M.; Rogers, J. A. Guided Growth of Large-Scale, Horizontally Aligned Arrays of Single-Walled Carbon Nanotubes and Their Use in Thin-Film Transistors. *Small* **2005**, *1*, 1110–1116.
9. Ishigami, N.; Ago, H.; Imamoto, K.; Tsuji, M.; Iakoubovskii, K.; Minami, N. Crystal Plane Dependent Growth of Aligned Single-Walled Carbon Nanotubes on Sapphire. *J. Am. Chem. Soc.* **2008**, *130*, 9918–9924.
10. Meitl, M. A.; Zhou, Y. X.; Gaur, A.; Jeon, S.; Usrey, M. L.; Strano, M. S.; Rogers, J. A. Transfer Printing Single-Walled Carbon Nanotube Films. *Nano Lett.* **2004**, *4*, 1643–1647.
11. Krupke, R.; Linden, S.; Rapp, M.; Hennrich, F. Thin Films of Metallic Carbon Nanotubes Prepared by Dielectrophoresis. *Adv. Mater.* **2006**, *18*, 1468–1470.
12. Li, X. L.; Zhang, L.; Wang, X. R.; Shimoyama, I.; Sun, X. M.; Seo, W. S.; Dai, H. J. Langmuir–Blodgett Assembly of Densely Aligned Single-Walled Carbon Nanotubes from Bulk Materials. *J. Am. Chem. Soc.* **2007**, *129*, 4890–4891.
13. Dittmer, S.; Svensson, J.; Campbell, E. E. B. Electric Field Aligned Growth of Single-Walled Carbon Nanotubes. *Curr. Appl. Phys.* **2004**, *4*, 595–598.
14. Ibrahim, I.; Bachmatiuk, A.; Börrnert, F.; Blüher, J.; Zhang, S.; Wolff, U.; Büchner, B.; Cuniberti, G.; Rümmeli, M. H. Optimizing Substrate Surface and Catalyst Conditions for High Yield Chemical Vapor Deposition Grown Epitaxially Aligned Single-Walled Carbon Nanotubes. *Carbon* **2011**, *49*, 5029–5037.
15. Brukh, R.; Sae-Khow, O.; Mitra, S. Stabilizing Single-Walled Carbon Nanotubes by Removal of Residual Metal Catalysts. *Chem. Phys. Lett.* **2008**, *459*, 149–152.
16. Nel, A.; Xia, T.; Mädler, L.; Li, N. Toxic Potential of Materials at the Nanolevel. *Science* **2006**, *311*, 622–627.
17. Nasibulin, A. G.; Pikhitsa, P. V.; Jiang, H.; Kauppinen, E. I. Correlation between Catalyst Particle and Single-Walled Carbon Nanotube Diameters. *Carbon* **2005**, *43*, 2251–2257.
18. Takagi, D.; Kobayashi, Y.; Homma, Y. Carbon Nanotube Growth from Diamond. *J. Am. Chem. Soc.* **2009**, *131*, 6922–6923.
19. Yao, Y.; Feng, C.; Zhang, J.; Liu, Z. "Cloning" of Single-Walled Carbon Nanotubes *via* Open-End Growth Mechanism. *Nano Lett.* **2009**, *9*, 1673–1677.
20. Rao, F.; Li, T.; Wang, Y. Growth of "All-Carbon" Single-Walled Carbon Nanotubes from Diamonds and Fullerenes. *Carbon* **2009**, *4*, 3580–3584.
21. Yu, X.; Zhang, J.; Choi, W.; Choi, J.-Y.; Kim, J. M.; Gan, L.; Liu, Z. Cap Formation Engineering: From Opened C-60 to Single-Walled Carbon Nanotubes. *Nano Lett.* **2010**, *10*, 3343–3349.
22. Lin, J.-H.; Chen, C.-S.; Rümmeli, M. H.; Zeng, Z.-Y. Self-Assembly Formation of Multi-Walled Carbon Nanotubes on Gold Surfaces. *Nanoscale* **2010**, *2*, 2835–2840.
23. Lin, J. H.; Chen, C. S.; Rümmeli, M. R.; Bachmatiuk, A.; Zeng, Z. Y.; Ma, H. L.; Büchner, B.; Chen, C. W. Growth of Carbon Nanotubes Catalyzed by Defect-Rich Graphite Surfaces. *Chem. Mater.* **2011**, *23*, 1637–1639.
24. Rümmeli, M. H.; Borowiak-Palen, E.; Gemming, T.; Pichler, T.; Knupfer, M.; Kalbac, M.; Dunsch, L.; Jost, O.; Silva, S. R. P.; Pompe, W.; *et al.* Novel Catalysts, Room Temperature, and the Importance of Oxygen for the Synthesis of Single-Walled Carbon Nanotubes. *Nano Lett.* **2005**, *5*, 1209–1215.
25. Rümmeli, M. H.; Schäffel, F.; Kramberger, C.; Gemming, T.; Bachmatiuk, A.; Kalenczuk, R. J.; Rellinghaus, B.; Büchner, B.; Pichler, T. Oxide-Driven Carbon Nanotube Growth in Supported Catalyst CVD. *J. Am. Chem. Soc.* **2007**, *129*, 15772–15773.
26. Kumar, M.; Ando, Y. Chemical Vapor Deposition of Carbon Nanotubes: A Review on Growth Mechanism and Mass Production. *J. Nanosci. Nanotechnol.* **2010**, *10*, 3739–3758.
27. Huang, S.; Cai, X.; Liu, J. Growth of Millimeter-Long and Horizontally Aligned Single-Walled Carbon Nanotubes on Flat Substrates. *J. Am. Chem. Soc.* **2003**, *125*, 5636–5637.
28. Ismach, A.; Joselevich, E. Orthogonal Self-Assembly of Carbon Nanotube Crossbar Architectures by Simultaneous Graphoepitaxy and Field-Directed Growth. *Nano Lett.* **2006**, *6*, 1706–1710.
29. Ruoff, R. S.; Tse, D. S.; Malhotra, R.; Lorents, D. C. Solubility of Fullerene (C_{60}) in a Variety of Solvents. *J. Phys. Chem.* **1993**, *97*, 3379–3383.
30. Huang, S.; Woodson, M.; Smalley, R.; Liu, J. Growth Mechanism of Oriented Long Single Walled Carbon

Nanotubes Using Fast-Heating Chemical Vapor Deposition Process. *Nano Lett.* **2004**, *4*, 1025–1028.
31. Biniaka, S.; Szymański, G.; Siedlewskia, J.; Światkowski, A. The Characterization of Activated Carbons with Oxygen and Nitrogen Surface Groups. *Carbon* **1997**, *35*, 1799–1810.
32. Jorio, A.; Saito, R.; Hafner, J. H.; Lieber, C. M.; Hunter, M.; McClure, T.; Dresselhaus, G.; Dresselhaus, M. S. Structural (n,m) Determination of Isolated Single-Walled Carbon Nanotubes by Resonant Raman Scattering. *Phys. Rev. Lett.* **2001**, *86*, 1118–1121.
33. Wang, H.; Luo, J.; Robertson, A.; Ito, Y.; Yan, W.; Lang, V.; Zaka, M.; Schäffel, F.; Rümmeli, M. H.; Briggs, G. A. D.; *et al.* High-Performance Field Effect Transistors from Solution Processed Carbon Nanotubes. *ACS Nano* **2010**, *4*, 6659–6664.
34. Wang, W. M.; LeMieux, M. C.; Selvarasah, S.; Dokmeci, M. R.; Bao, Z. Dip-Pen Nanolithography of Electrical Contacts to Single-Walled Carbon Nanotubes. *ACS Nano* **2009**, *3*, 3543–3551.
35. Zhou, X. J.; Park, J. Y.; Huang, S. M.; Liu, J.; McEuen, P. L. Band Structure, Phonon Scattering, and the Performance Limit of Single-Walled Carbon Nanotube Transistors. *Phys. Rev. Lett.* **2005**, *95*, 146805.
36. Ho, X. N.; Ye, L. N.; Rotkin, S. V.; Cao, Q.; Unarunotai, S.; Salamat, S.; Alam, M. A.; Rogers, J. A. Scaling Properties in Transistors That Use Aligned Arrays of Single-Walled Carbon Nanotubes. *Nano Lett.* **2010**, *10*, 499–503.
37. Kang, S. J.; Kocabas, C.; Ozel, T.; Shim, M.; Pimparkar, N.; Alam, M. A.; Rotkin, S. V.; Rogers, J. A. High-Performance Electronics Using Dense, Perfectly Aligned Arrays of Single-Walled Carbon Nanotubes. *Nat. Nanotechnol.* **2007**, *2*, 230–236.
38. Yao, Z.; Kane, C. L.; Dekker, C. High-Field Electrical Transport in Single-Wall Carbon Nanotubes. *Phys. Rev. Lett.* **2000**, *84*, 2941–2944.
39. Kane, C. L.; Mele, E. J.; Lee, R. S.; Fischer, J. E.; Petit, P.; Dai, H.; Thess, A.; Smalley, R. E.; Verschueren, A. R. M.; Tans, S. J.; *et al.* Temperature-Dependent Resistivity of Single-Wall Carbon Nanotubes. *Europhys. Lett.* **1998**, *41*, 683–688.
40. Ando, T.; Nakanishi, T. Impurity Scattering in Carbon Nanotubes—Absence of Back Scattering. *J. Phys. Soc. Jpn.* **1998**, *67*, 1704–1713.
41. Lazzeri, M.; Mauri, F. Coupled Dynamics of Electrons and Phonons in Metallic Nanotubes: Current Saturation from Hot Phonons Generation. *Phys. Rev. B* **2006**, *73*, 165419:1−6.
42. Park, J.-Y.; Rosenblatt, S.; Yaish, Y.; Sazonova, V.; Ustünel, H.; Braig, S.; Arias, T. A.; Brouwer, P. W.; McEuen, P. L. Electron−Phonon Scattering in Metallic Single-Walled Carbon Nanotubes. *Nano Lett.* **2004**, *4*, 517–520.
43. Nemec, N.; Tománek, D.; Cuniberti, G. Modeling Extended Contacts for Nanotube and Graphene Devices. *Phys. Rev. B* **2008**, *77*, 125420:1−12.
44. Tabata, H.; Shimizu, M.; Ishibashi, K. Fabrication of Single Electron Transistors Using Transfer-Printed Aligned Single-Walled Carbon Nanotubes Arrays. *Appl. Phys. Lett.* **2009**, *95*, 113107-1-3.